Where Quantum and Fluids entangle

Quantum Computational Fluid Dynamics
Core Set Of Examples and Solutions
Project number 101080085

Call:	HORIZON-CL4-2021-DIGITAL-EMERGING-02
Topic:	HORIZON-CL4-2021-DIGITAL-EMERGING-02-10
Type of action:	HORIZON Research and Innovation Actions
Granting authority:	European Commission-EU
Project starting date: fixed date:	1 November 2022
Project end date:	31 October 2026
EU-Project duration:	48 months
Project Coordinator:	University of Hamburg (UHH)
Work Package Leader	Forschungszentrum Juelich (FZJ)
Cooperations	Technical University of Crete (TUC), University of Hamburg (UHH)
Deliverable number:	D7.1
WP contributing to the deliverable:	WP#7 Flagship hardware calculations
Deliverable Type:	Data
Revision:	0
Dissemination level:	Public
Due Submission date:	31.01.2025
Prepared By:	FZJ, TUC, PLANQC
Internal Reviewers:	DJ, DA, MK
Final Approval:	DJ

This project receives funding from the European Union's Horizon 2020 HORIZON Research and Innovation Actions Programme under Grant Agreement #101080085

Revision History

Version	Date	Who	Changes
R0	30.01.2025	FM	

This project receives funding from the European Union's Horizon 2020 HORIZON Research and Innovation Actions Programme under Grant Agreement #101080085

List of abbreviations

Acronym / Short Name	Meaning
CA	Consortium Agreement
CFD	Computational Fluid Dynamics
CFL	Courant-Friedrichs-Levy criteria
D	Deliverable
DMP	Data Management Plan
DOI	Digital Object Identifier
EC	European Commission
ENG	ENGYS SRL
EU	European Union
FD	Finite Difference
FDR	Research Data Repository
FV	Finite Volume
FZL	Jülich Research Centre
KPI	Key Performance Indicator
LES	Large-Eddy Simulation
PlanQc	PlanQc GMBH
PO	Project Officer
QCFD	Quantum Computational Fluid Dynamics
VQA	Variational Quantum Algorithm
TUHH	Technical University of Hamburg
TUC	Technical University of Crete
TUM	Technical University of Munich
UHH	University of Hamburg
WP	Work Package
WPL	Work Package Leader

This project receives funding from the European Union's Horizon 2020 HORIZON Research and Innovation Actions Programme under Grant Agreement #101080085

1 Executive Summary

The Quantum Computational Fluid Dynamics (QCFD) project is dedicated to establishing an open-access quantum software framework to address Computational Fluid Dynamics (CFD) challenges present in today's industry.

As a part of the Work Package 7 (WP7) "Flagship hardware calculations", Deliverable D7.1 provides a core set of "small benchmark" examples of solutions computed with quantum circuit gate-level simulations and first usage of quantum hardware. These problems are simplified to be able to run on current and short term capabilities of quantum computers, and provide a basis for comparison with benchmark CFD solutions from work packages 1, 4, and 6.

In accordance with the Data Management Plan (DMP), D7.1 follows the FAIR data principles – Findability, Accessibility, Interoperability, and Reusability – where each dataset is provided with a detailed metadata structure with unique identifiers and proper documentation, ensuring that the data is not only easily accessible but also readily transferable and reusable. The access to the public is granted by a dedicated research data repository (FDR) hosted at the university of Hamburg (UHH), https://www.fdr.uni-hamburg.de/communities/qcfd/. To facilitate the users overview, all datasets belonging to the QCFD project, namely those from this report (which include 10.25592/uhhfdm.16681, 10.25592/uhhfdm.16690, 10.25592/uhhfdm.16718, 10.25592/uhhfdm.16129, and 10.25592/uhhfdm.16108) are collected in a QCFD community group on the mentioned data server.

This project receives funding from the European Union's Horizon 2020 HORIZON Research and Innovation Actions Programme under Grant Agreement #101080085

Contents

1 Executive Summary **4**

2 Introduction **6**

3 Platforms **6**

4 Data Organization **7**

5 Nonlinear Schrodinger Equation **7**

6 Burgers' Equation **10**
6.1 Mitigation Strategies 11
6.2 Preliminary IBM results 11
6.2.1 Tiling 11
6.2.2 Sherbrooke 12
6.2.3 Future Directions 13
6.3 Emulation on PlanQC simulator 15

7 European Hardware **16**
7.1 Experiments planned upon scheduled hardware availability 16
7.2 Improvement feedback 16

8 Summary **17**

This project receives funding from the European Union's Horizon 2020 HORIZON Research and Innovation Actions Programme under Grant Agreement #101080085

2 Introduction

Solving numerically differential equations is at the heart of science and engineering because many fundamental processes in nature are described by such equations. Examples include the convection-diffusion process, wave dynamics, fluid dynamics to name a few [1]. The typical approach for solving these equations is to discretize the solution candidate in position and time and write the derivatives (variations) using approximate methods such as finite difference and solve the differential equation iteratively [2]. The main problem with this approach relies on the increasing number of resources for simulating these systems up to a bounded precision, requiring high-parallelization and high-performance computing.

Therefore new computational technologies are required. One possible approach relies on using quantum computers, where it has been proposed that solving algorithms on them may lead to better asymptotic scaling, when compared with its classical counterpart [3, 4]. In this framework, we can exploit the elements from gate-based quantum computation for encoding the required operations (time and spatial derivative) and variational quantum circuits [5] for engineering adequate candidates (anzätzes) of the solution. Both problems (operation and anzatz) are mapped to quantum circuits that can be run on an operative quantum computer. Nowadays, there are a wide range of potential quantum computers running with a modest number of qubits in the so-called Noise Intermediate-Scale Quantum Computers (NISQ) [6] from different platform such as photons [7], neutral atoms [8], trapped-ions [9] and superconducting circuits [10, 11]. Each of them has its own strengths and disadvantages that can exploited to solve differential equations. For this deliverable, provide an early exploration of the necessary elements in order to successfully solve these equations on a superconducting quantum computer.

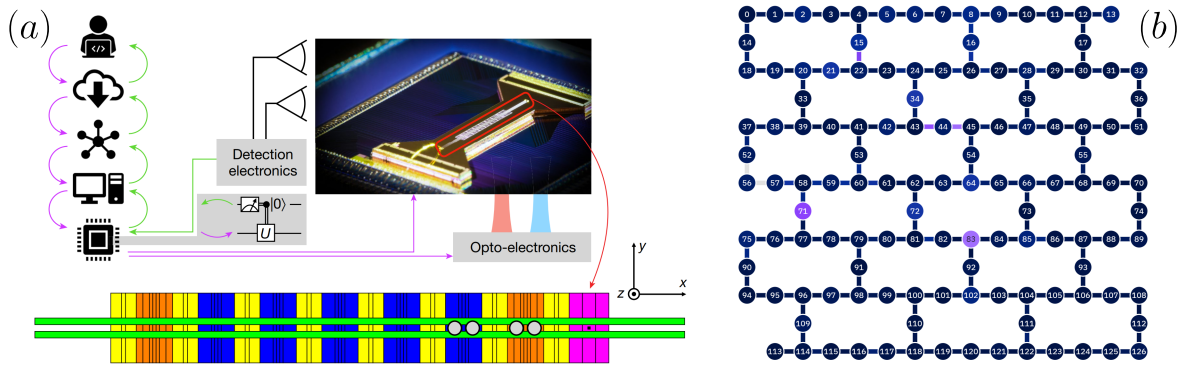

Figure 1: Representation of a Trapped Ion Computer (a) from [12] and an IBM 127 superconducting qubits quantum Computers(b) from [11]. Whilst the Ion trap allows for all-to-all connectivity, the superconducting computer possesses a limited topology, where only certain connections between qubits are allowed.

3 Platforms

Following the conclusions of **workpackage report 6.1**, we focus on superconducting qubits due to their high rate of measurement and circuit speed, a necessary condition to achieve the desired precision for this algorithm. We analysed the simulated performances of the IBM superconducting quantum processors `Sherbrooke`. The processor consist of 127 Transmon qubits [13] capacitively connected to auxiliary resonators on a grid configuration [dark blue lines on Fig. 1(b)]. The IBM architecture does not support *all-to-all* connectivity. To perform operations between distant qubits swap operations are needed, increasing the overhead of the circuit. In this architecture, both single- and two-qubit operations are implemented by voltage-controlled microwave drives addressing one [14] or both qubits at the same time [15, 16]. Finally, the readout of the qubit is performed using an auxiliary resonator so that the measured voltage is proportional to the state of the qubit [17, 18]. For these architectures, the native set of gates are the following

- Single-qubit gates

$$\sqrt{X} = \frac{1}{2}\begin{pmatrix} 1+i & 1-i \\ 1-i & 1+i \end{pmatrix}, \quad X = \begin{pmatrix} 0 & 1 \\ 1 & 0 \end{pmatrix}, \quad \mathrm{RZ}(\lambda) = \begin{pmatrix} e^{-i\frac{\lambda}{2}} & 0 \\ 0 & e^{i\frac{\lambda}{2}} \end{pmatrix}. \tag{1}$$

This project receives funding from the European Union's Horizon 2020 HORIZON Research and Innovation Actions Programme under Grant Agreement #101080085

- Two-qubit gates

$$\text{ECR} = \frac{1}{\sqrt{2}} \begin{pmatrix} 0 & 0 & 1 & i \\ 0 & 0 & i & 1 \\ 1 & -i & 0 & 0 \\ -i & 1 & 0 & 0 \end{pmatrix} \tag{2}$$

Qubit	**Readout**	**ID**	$\sqrt{X}$	**Pauli-X**	**ECR**
0	4.80	2.008	2.008	2.008	1_0:0.0134
1	2.13	3.565	3.565	3.565	1_2:0.0095
2	5.40	2.633	2.633	2.633	1_0:0.0134
3	1.30	2.214	2.214	2.214	3_2:0.0089
4	1.72	1.618	1.618	1.618	4_3:0.0046
5	4.61	2.933	2.933	2.933	5_4:0.0072

Table 1: Error sources (in %) of the Sherbrooke IBM quantum processor.

All these operations are affected by the action of the electronic environment that introduces relaxation, decoherence and crosstalk [19]. The typical errors affecting the architecture are summarized in Table 1.

4 Data Organization

Following the model of previous reports, we maintain the same guidelines for data accuracy and transparency. Therefore, for each equation analysed we provide the parameters and field obtained at each time step in easily readable files either in `.txt` format or `.npy` format. All data is clearly labeled and indicated in the appropriate file. All numbers are used with double-precision floating-point number format. Data obtained from experiments on IBM machines is provided in `.csv` format.

To access the data obtained throughout this report we mainly used two criteria: **Fidelity** - the similarity measure and formed by the scalar product of two normalized vectors - and the **Mean Squared Error** - an average measure of the squared difference between two data sets.

5 Nonlinear Schrodinger Equation

The nonlinear Schrödinger equation (NLSE) and its variants model various phenomena [20, 21, 22, 23, 24, 25, 26, 27, 28, 29], such as dynamics of light in nonlinear optics [22, 23], envelope solitons and modulation instabilities in plasma physics and surface gravity waves [24], and characteristics including superfluidity and vortex formation in Bose-Einstein Condensates (BEC) [25, 26, 27, 28, 29], to name a few. In dimensionless form, the time-independent NLSE is given as

$$\left[-\frac{1}{2}\frac{d^2}{dx^2} + V(x) + gI_{f(x)} \right] f(x) = Ef(x) \, . \tag{3}$$

Here, $f(x)$, with x being spatial coordinates, represents a normalized single real-valued function defined over the interval $[a, b]$. The term $I_{f(x)}$ represents the nonlinear interaction, g denotes the strength of the nonlinearity, and $V(x)$ is the external potential. In this study, we consider $I_{f(x)} = |f(x)|^2$, quadratic potential $V(x) = V_0(x - x_0)^2$ centered around $x_0 = \frac{b-a}{2}$, and periodic boundary conditions such that $f(b) = f(a)$ and $V(b) = V(a)$. Small instances of the Eq. (3) can be solved numerically on classical computers by employing imaginary-time evolution [30, 27], spectral, variational or other methods [20]. However, when addressing large instances of nonlinear problems, the limitations associated with memory capacity and computational time inherent in classical computation become increasingly apparent.

By applying the finite-difference method, the expectation value of the total energy [from Eq. (3)] of the system is given as the sum of potential, interaction, and kinetic energies, $\langle\langle E\rangle\rangle = \langle\langle E_P\rangle\rangle + \langle\langle E_I\rangle\rangle + \langle\langle E_K\rangle\rangle$, where

$$\langle\langle E_P\rangle\rangle = \sum_{k=0}^{N-1} |\psi_k|^2 V_k \, , \qquad \langle\langle E_I\rangle\rangle = \sum_{k=0}^{N-1} \frac{g}{\delta} |\psi_k|^4 ,$$

$$\langle\langle E_K\rangle\rangle = -\frac{1}{2\delta^2} \sum_{k=0}^{N-1} \left(\psi_k^* \psi_{k+1} - 2\psi_k^* \psi_k + \psi_k^* \psi_{k-1} \right),$$

This project receives funding from the European Union's Horizon 2020 HORIZON Research and Innovation Actions Programme under Grant Agreement #101080085

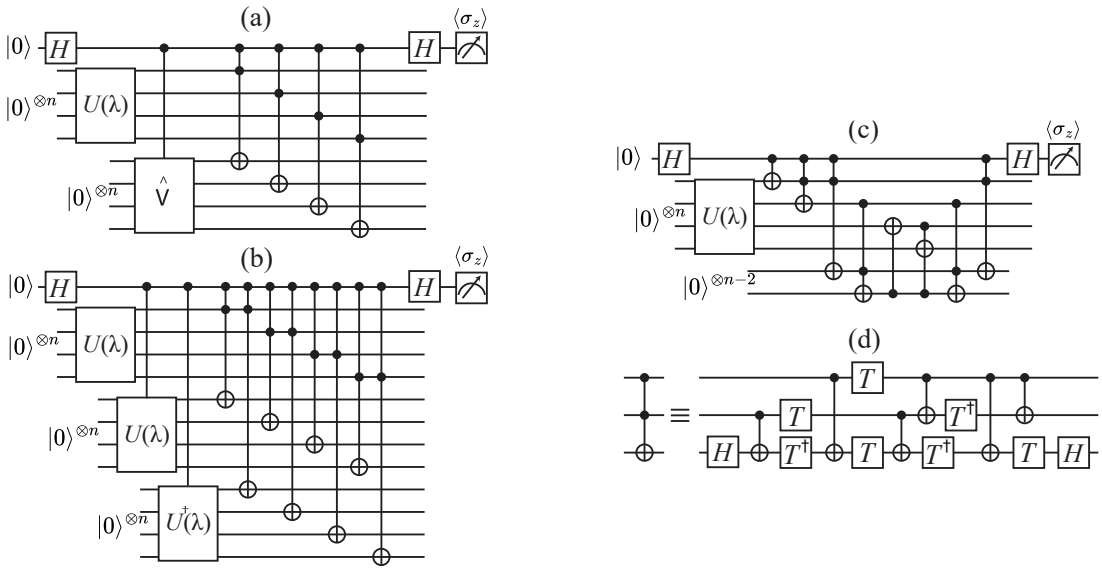

Figure 2: Design of the quantum circuits used to measure the (a) potential, (b) interaction, and (c) kinetic energies. Here, H is the Hadamard gate, $U(\lambda)$ is the quantum ansatz that represents the trial state, and $\hat{V}$ is the potential unitary which encodes the potential function values to the basis states. Here, we have shown an example of $n = 4$ ($n' = 13$), which can be generalized to an arbitrary number of qubits. Panel (d) shows the decomposition of the Toffoli gate into a sequence of single-qubit gates and controlled-NOT gates, where $T = R_z(\pi/4)$ and $T^{\dagger} = R_z(-\pi/4)$

for the discretized problem and $\langle\langle \cdots \rangle\rangle$ represent the expectation value [31]. We consider the total energy as the cost function $\mathcal{C} = \sum_j \mathcal{C}_j = \sum_j \langle\langle E_j \rangle\rangle$ for the variational algorithm such that the minimum value of the cost function represents the ground state solution. Figure 2 depicts the quantum circuits to evaluate the kinetic, potential and interaction energies.

The group at TUC implemented (see arXiv:2403.16426) the circuits on the digital gate-based quantum devices, `ibmq-mumbai` and `ibmq-kolkata`, both of which feature identical topology and basis gate sets. These two devices were selected due to their availability and our limited access to IBMQ processors. The target is $n = 2$ ($n' = 7$) qubit system with $g = 5000$ and design the quantum ansatz tailored to the strong nonlinearity case, such that each qubit has a Hadamard gate followed by a layer of parameterized single-qubit R_y rotation gate, as shown in Fig. 3(a). It is important to highlight that our goal here is to analyze the performance of evaluating the cost function on the quantum devices; therefore, we restrict the variational space, which might not include the exact ground state. The simplified ansatz of Fig. 3(a) offers two advantages. The first advantage is the absence of CNOT gates, resulting in quantum circuits with fewer entangling gates and a shallow circuit depth. Consequently, the quantum circuits to measure kinetic, potential, and interaction energies consist of 14, 59, and 70 (33, 160, and 124) CNOT (single-qubit) gates, respectively. The second advantage is that, for the zero value of each variational parameter, the quantum ansatz generates a trial state with over 99% fidelity with the exact ground state in the strong nonlinearity regime. This insight allows us to restrict the variational space closer to the ground state, such that even for the non-zero but smaller values of the variational parameters, the trial state maintains considerable overlap with the ground state. With this setting, we execute the variational algorithm in the presence of hardware noise, where each parameter of the ansatz is initiated at zero value (red point in Fig. 3(b)). The classical optimizer explores the two-dimensional variational space for a few iterations before converging toward the zero values of the variational parameters (a green point in Fig. 3(b) indicates the set of final values of the variational parameters).

With these pre-trained quantum circuits, we measure the energy cost function and fidelity of state probabilities in both noiseless simulations and noisy settings of simulations and digital quantum hardware. It is worth noting that, unlike the noisy simulations, quantum hardware simulations exhibit qubit reset noise. Fig. 3(d) demonstrates the percentage fidelity $\%F = (1 - \sum_{k=0}^{2^n-1} \left[|\psi_{\rm GS}|^2 - |\psi_{\rm var,k}|^2\right]) \times 100$ of the trial state probabilities with a maximum disparity of 0.25% between noiseless simulations and quantum device simulations, highlighting the high-fidelity preparation of the trial state across the two devices. Additionally, the evaluation of the energy cost function and components in both noiseless (depicted in

This project receives funding from the European Union's Horizon 2020 HORIZON Research and Innovation Actions Programme under Grant Agreement #101080085

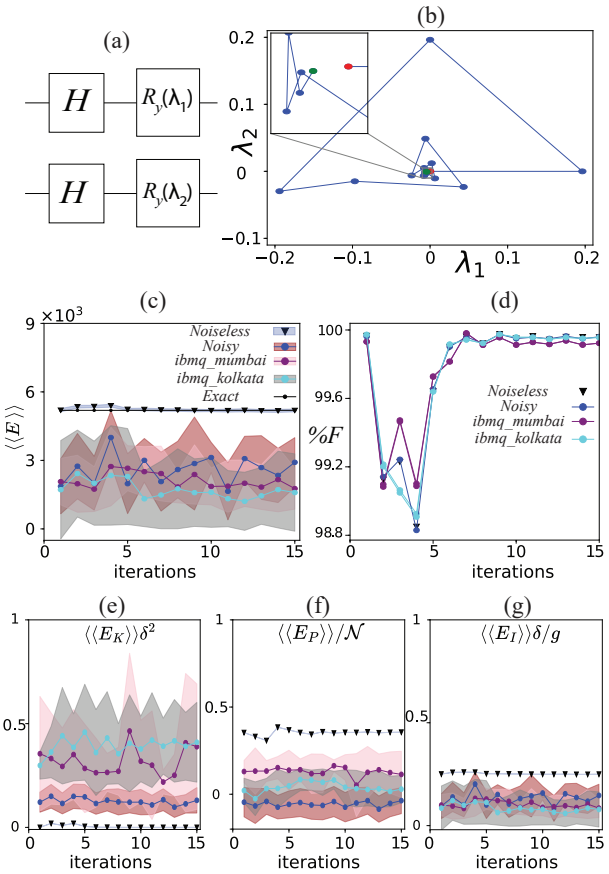

Figure 3: The performance of evaluating the cost function on IBM Q devices. Panel (a) shows the simplified quantum ansatz adopted for the quantum device demonstration of the variational algorithm. Panel (b) represent the training of variational parameters, where red (green) marker highlight the initial (final) point of the classical optimization. Panel (c) shows the energy $\langle\langle E\rangle\rangle_{\text{var}}$ vs iterations of classical optimizer for $g = 5000$, $n = 2$ ($n' = 7$). Here, blue (black) color indicate the noisy (noiseless) simulations, while purple and cyan colors represent simulations performed on `ibmq-mumbai` and `ibmq-kolkata` devices, respectively. Moreover, the blue, brown, pink, and gray colors highlight the region of one standard deviation. Panel (d) shows the fidelity $\%F = (1 - \sum_{k=0}^{2^n-1} \left[|\psi_{\text{GS}}|^2 - |\psi_{\text{var,k}}|^2\right]) \times 100$ of the trial state probabilities with respect to the ground state solution. Panel (e, f, g) shows the quantities $\langle\langle E_K\rangle\rangle\delta^2$, $\langle\langle E_P\rangle\rangle/\mathcal{N}$, and $\langle\langle E_I\rangle\rangle\delta/g$, and corresponding standard deviations.

black) and noisy (depicted in blue) simulations, as shown in Figs. 3(c), 3(e-g), aligns with the findings presented in Report 6.1, with differences and variances stemming from the impact of quantum noise.

Figs. 3(c) and 3(e-g) show the energy cost function and individual components measured on the `ibmq-mumbai` (in purple color) and `ibmq-kolkata` (in cyan color) devices. The results exhibit behavior akin to those observed in the noisy simulations. Here, the qubit reset noise, causing imperfect initialization of ancillary qubits and quantum registers, further impacts the encoding (preparation) of the potential function (variational state) and the execution of the adder circuit, resulting in significant increases in standard deviation values. These findings reveal large errors and variances, thereby highlighting the limitations of the current NISQ devices in executing the variational algorithm for nonlinear cost functions.

Data presented here regarding hardware implementation is available at DOI 10.25592/uhhfdm.16680 while the comparison with classical emulation of noisy quantum hardware is provided at 10.25592/uhhfdm.16129.

This project receives funding from the European Union's Horizon 2020 HORIZON Research and Innovation Actions Programme under Grant Agreement #101080085

6 Burgers' Equation

Another problem tackled so far is the Burgers' Equation. It is an object of great interest because it is the simplest model where we can observe non-linear effects in fluids such as shockwaves, turbulences and traffic flow due to the competition between diffusion and the non-linear convection. Its one dimensional form reads

$$\frac{\partial u(x,t)}{\partial t} = u(x,t)\frac{\partial u(x,t)}{\partial x} + \nu\frac{\partial^2 u(x,t)}{\partial x^2}, \tag{4}$$

where $u(x,t)$ is the spatiotemporal distribution of the velocity field of the fluid. ν represents the viscosity of the fluid. We solve this equation by discretizing both position and time. We use the Euler method to discretize in time:

$$\frac{\partial u(x,t)}{\partial t} = \frac{u(x_i, t_j + dt) - u(x_i, t_j)}{dt}. \tag{5}$$

and the final central difference to discretize in space:

$$\nu\frac{\partial^2 u(x,t)}{\partial x^2} = \nu\left[\frac{u(x_i + dx, t_j) - 2u(x_i, t_j) + u(x_i - dx, t_j)}{(dx)^2}\right] \tag{6}$$

$$u(x,t)\frac{\partial u(x,t)}{\partial x} = u(x_i, t_j)\frac{u(x_{i+1}, t_j) - u(x_{i-1}, t_j)}{2dx}, \tag{7}$$

To fulfill the normalization of the wave function we use an extra parameter:

$$u(x, t_j) = \lambda_j^0 U(\vec{\theta}_j)|\bar{\mathbf{0}}\rangle, \tag{8}$$

This equation translates into five measurements:

$$E_1 = \left[1 - 2\nu\frac{dt}{(dx)^2}\right]\langle\bar{\mathbf{0}}|\hat{\mathbf{U}}^\dagger(\vec{\theta}_j)\hat{\mathbf{U}}(\vec{\theta}_{j+1})|\bar{\mathbf{0}}\rangle, \tag{9a}$$

$$E_2 = \nu\frac{dt}{(dx)^2}\left[\langle\bar{\mathbf{0}}|\hat{\mathbf{U}}^\dagger(\vec{\theta}_j)\hat{\mathbf{A}}\hat{\mathbf{U}}(\vec{\theta}_{j+1})|\bar{\mathbf{0}}\rangle + \langle\bar{\mathbf{0}}|\hat{\mathbf{U}}^\dagger(\vec{\theta}_j)\hat{\mathbf{A}}^\dagger\hat{\mathbf{U}}(\vec{\theta}_{j+1})|\bar{\mathbf{0}}\rangle\right], \tag{9b}$$

$$E_3 = \lambda_{j+1}^0\frac{dt}{2dx}\left[\langle\bar{\mathbf{0}}|\hat{\mathbf{U}}^\dagger(\vec{\theta}_j)\tilde{\mathbf{D}}^\dagger\mathbf{A}\hat{\mathbf{U}}(\vec{\theta}_{j+1})|\bar{\mathbf{0}}\rangle - \langle\bar{\mathbf{0}}|\hat{\mathbf{U}}^\dagger(\vec{\theta}_j)\tilde{\mathbf{D}}^\dagger\hat{\mathbf{A}}^\dagger\hat{\mathbf{U}}(\vec{\theta}_{j+1})|\bar{\mathbf{0}}\rangle\right]. \tag{9c}$$

where E_1 emerges from the time derivative and the Laplacian, E_2 from the remaining terms in the Laplacian and E_3 from the convection term.

The cost function to evaluate will be:

$$C(\lambda_{j+1}^0, \vec{\theta}_j) = |\lambda_j^0|^2 + |\lambda_{j+1}^0|^2 - 2\lambda_{j+1}^0\lambda_j^0(E_1 + E_2 + E_3), \tag{10}$$

As in the 6.1 work package report, the results presented in this section are quantified using the Mean Squared Error (MSE) metric and the respective standard deviation (σ):

$$\mathrm{MSE}_j = \frac{1}{N}\sum_i^N [u^{\mathrm{C}}(x_i, t_j) - u^{\mathrm{Q}}(x_i, t_j)]^2 \tag{11}$$

where $u^{\mathrm{C}}(x_i, t_j)$ and $u^{\mathrm{Q}}(x_i, t_j)$ are the classical and quantum solutions, respectively.

$$\sigma = \sqrt{\frac{1}{N}\sum_i^{N=10}(\mathrm{MSE}_i - \overline{\mathrm{MSE}})^2} \tag{12}$$

This project receives funding from the European Union's Horizon 2020 HORIZON Research and Innovation Actions Programme under Grant Agreement #101080085

6.1 Mitigation Strategies

An intrinsic property of NISQ devices running algorithm and quantum circuits are its fragility against coherent and incoherent errors. While the former can be corrected using optimal quantum control or machine learning techniques, the latter can not be fully corrected but instead they can be mitigated. Nowadays, mitigation procedures require running the same circuit several times in order to characterize and remove the accumulated error in the hardware allowing us to achieve solutions that are resistant against the decoherence/depolarization errors.

Thus, we use the Zero Noise Extrapolation (ZNE) mitigation technique [32] to our circuits. Roughly speaking, ZNE consists in evaluating an expectation value of our interest at different noise values to extract the ideal (noiseless) one inferred by extrapolating the previous observable. We increase the noise level in our quantum circuit by applying gates that in the noiseless limit corresponds to the identity, but in the real implementation it accumulates errors. In the context of QCFD project, the largest sources of errors corresponds to the two-qubit gates - the CNOT gates. Given that applying two of them we get the identity, we increase the noise of our circuit by replacing each CNOT with three and then five CNOTs, respectively.

The results were then fitted to a quadratic curve. An example is shown in figure 4.

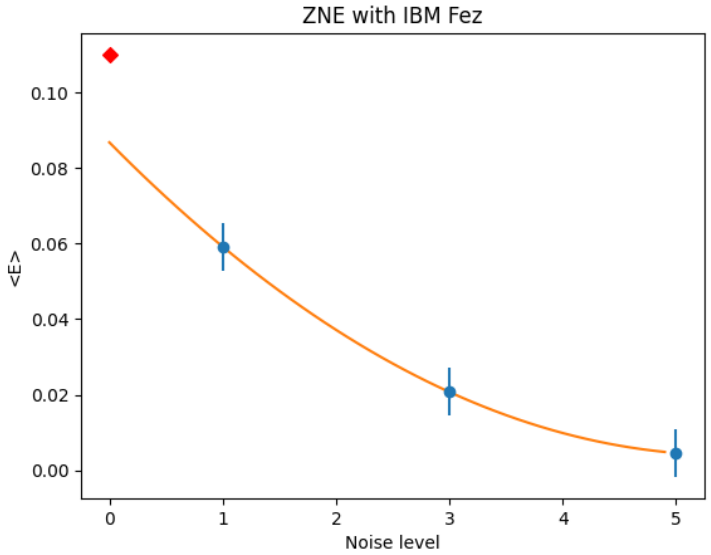

Figure 4: Example of Zero Noise extrapolation with a quadratic fit. The extrapolated value, 0.0867 is considerably closer to the ideal value, 0.110, than the measured value, 0.0592. We used IBM_Fez

When executing on IBM devices we further employ Pauli Twirling [33], a technique that allows us to tailor quantum noise so that ZNE is more effective, and Twirled Readout Error eXtinction (TREX) [34], a technique that reduces the biases introduced in expectation values due to error in measurements.

6.2 Preliminary IBM results

Armed with these techniques we moved on to the actual implementation of the Burger's equation on the IBM quantum platform. We set our parameters as $\nu = 0.01$ for the viscosity, and assume that the initial field distribution has a sinusoidal profile $u(x_k, 0) = \sin(2\pi x_k/N)$, where $N = 2^n$ is the discretization length. Given that NISQ devices are still noisy we encode the field in $n = 3$ qubits.

In order to mitigate the effect of the noise while running the variational algorithm, we demand that the circuit encoding the problem be as shallow as possible. In this direction, following the proposal in **workpackage 6.1**, we use an ansazt consisting of four parameters, four controlled rotations and two CNOTs. This Ansatz will require a minimum of 10 CNOTs and the necessary single-qubit operations to encode in a quantum computer.

6.2.1 Tiling

IBM cloud platform based on `qiskit` works by generating sessions, consisting in fixed amount on time for executing quantum circuits. In a preliminary stage, we aim to run sequentially our variational circuit

This project receives funding from the European Union's Horizon 2020 HORIZON Research and Innovation Actions Programme under Grant Agreement #101080085

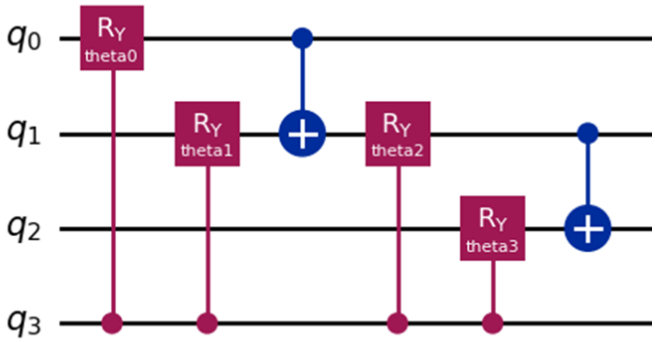

Figure 5: Ansatz to solve the Burgers' equation

with ZNE with a large amount of measurements i.e, we compute one part of the cost function at the time. As consequence, we run out the dedicated session time without finishing the time step. We circumvent this limitation by employing *Tiling* where we encode the different circuits of the cost function in a bigger one using all the resources of the hardware. We have used `qiskit transpiler` to select the best available qubits. The trade-off of this techniques relies in a substantial amount of time required in the session (approximately five-fold speedup) at the expenses of using qubits whose performance is more susceptible to coherent noise (lower two-qubit gate fidelities) and incoherent noise (loss of quantumness). Another consideration about the techniques is that as we are using a larger number of qubits from *8 to 32*, classical simulations are no longer accessible, making necessary the use of the real hardware. Fig 6 depicts an example of how do we implement the tiling method.

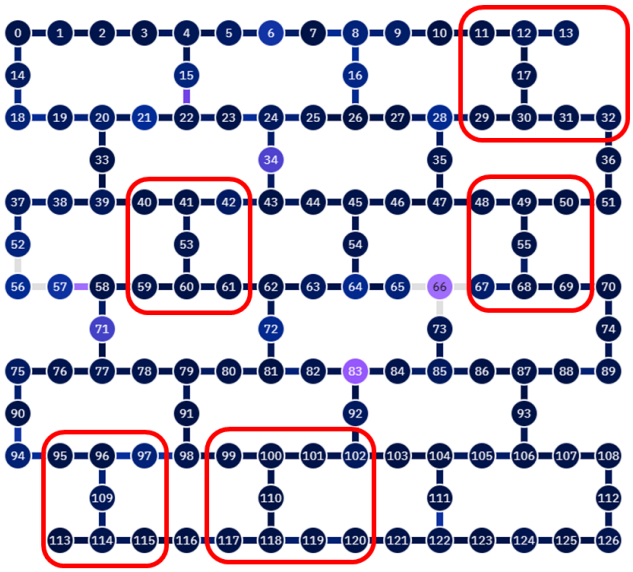

Figure 6: Example of the Tiling proposed in the hardware `IBM_fez` where we encode different circuits in different parts of the hardware (red blocks in the figure). Dark blue dots correspond to qubits with small readout errors.

6.2.2 Sherbrooke

Using this techniques we manage to run a single time step of 0.3 (s) on `ibmq-Sherbrooke`. The experiments were conducted from `25/08/2024` to `24/09/2024` spanning multiple calibrations of the device. The data obtained is available at the **workpackage repository**. We plot the field solution of the Burgers' equation in 7. By comparing with the classical solution, we obtain a MSE of 0.262.

This project receives funding from the European Union's Horizon 2020 HORIZON Research and Innovation Actions Programme under Grant Agreement #101080085

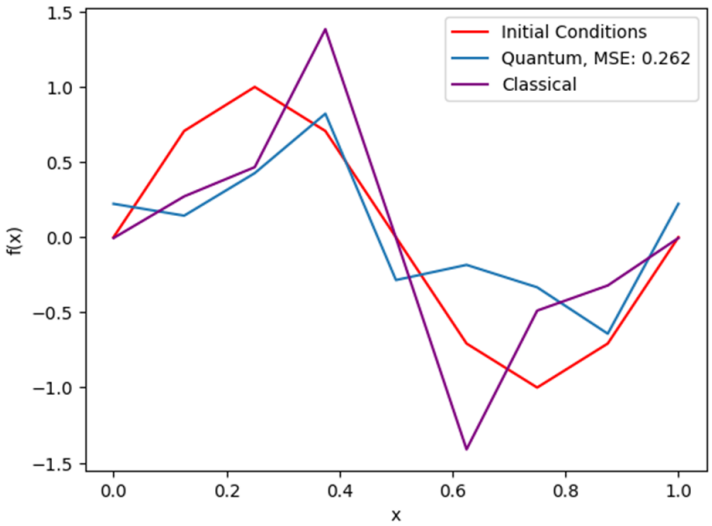

Figure 7: Field obtained from running the Algorithm on `ibmq-Sherbrooke` for a single time step $dt = 0.3$. The field itself was obtained by simulating the Ansatz with the parameters extracted from the quantum computer

We should mention that even though the achieved MSE is large, we can still observe nontrivial behavior in the fluid as the shock-wave given by the abrupt change of the field profile. This is to date the first prototype/evidence of quantum computer's capability to capture nontrivial properties of fluids by using variational algorithm for solving PDEs. Additionally, the presence of the shock-wave also demonstrates the capability of the hardware to produce a solution that is not just random noise even though the variational circuit has large depth with approximately 100 CNOTs gates, over different calibrations along the period where the experiments were conducted. Lastly, we have to point out that `ibmq-Sherbrooke` is not part of IBMs most cutting edge computers. Indeed, given the rapid development of the field new hardware have been made recently available based on a tunable architecture exhibiting high fidelities. Therefore, we can remain cautiously optimistic about future prospects for this project.

6.2.3 Future Directions

Given the results presented so far, we establish 3 important avenues to obtain a better solution to the Burgers' equation.

The first is to simply use better hardware. This obviously will help us achieve better results, but better hardware is a result of a massive research effort. Beyond using the latest machines made available by IBM, we are limited by the current available technology.

The second path consists in reducing the number of two-qubit gates used in the algorithm. To achieve this further reduction we focused in replacing the CRY gates, which are translated into 2 CNOT gates. These are replaced by a single qubit rotation by angle θ, a CNOT and an inverse rotation by angle $-\theta$ so that when the CNOT is not activated the action is just the identity. Although this does not reproduce the action of a CRY perfectly by introducing an extra parameter we can still generate a Hilbert space big enough to contain the solution to the equation. This change allows us to save 5 CNOTs in the Ansatz and for the deeper circuits it translates to a $\approx 20\%$ reduction in the number of two-qubit gates, after transpiling. The new ansatz can be seen in Fig. 8.

The third path forward consist in the application of new mitigation techniques. In that line, we followed the framework of [35] to extract more information regarding the action of noise over our circuit by making measurements before the second Hadamard gate over all qubits. This way, we can compare the fraction of measurements where all qubits remain in the $|0\rangle$ state with the fraction of measurements where only the control qubit remained in $|0\rangle$. Given that the majority of the noise comes from two-qubit gates, this fraction should be independent of the rotation parameters and of the Hadamard gates.

By doing this procedure, we can estimate how much of our system has left the desired state $|\psi\rangle\langle\psi|$. If we assume our noise is modeled by a depolarizing channel, the evolution of the system when the control qubit is in $|0\rangle$ will be:

This project receives funding from the European Union's Horizon 2020 HORIZON Research and Innovation Actions Programme under Grant Agreement #101080085

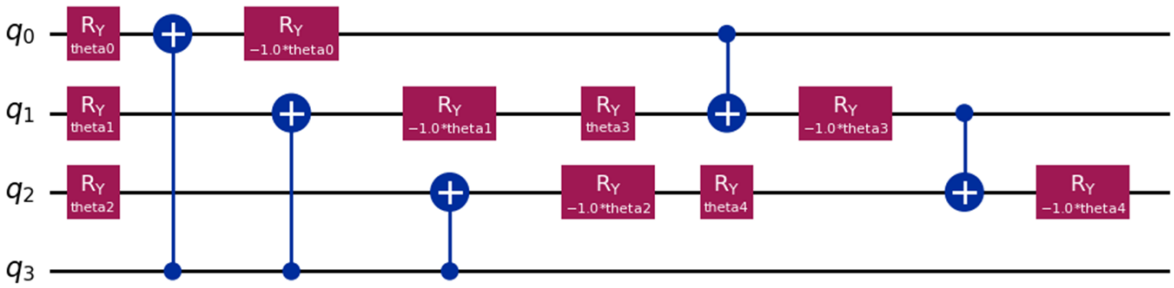

Figure 8: New Ansatz with only single gate rotations

$$|0_N\rangle\langle 0_N| \rightarrow (1-\lambda)|0_N\rangle\langle 0_N| + \frac{\lambda}{N^2}\mathbb{I} \tag{13}$$

and in the $|1\rangle$ will be:

$$|1_0\rangle|0_{N-1}\rangle\langle 0_{N-1}|\langle 1_0| \rightarrow (1-\lambda)|1_0\rangle|\psi\rangle\langle\psi|\langle 1_0| + \frac{\lambda}{N^2}\mathbb{I}, \tag{14}$$

where $\mathbb{I}$ represents the identity. Given that the identity will affect the probability of measuring $|0\rangle$ and $|1\rangle$ on the control qubit in the same way, in this model the effect of the noise on the expectation value of any operator will be to effectively reduce the measured result by a factor of $(1-\lambda)$:

$$\langle E\rangle_{\text{ideal}} = \frac{\langle E\rangle}{(1-\lambda)} \tag{15}$$

The factor $(1-\lambda)$ can now be extracted from the fraction of shots measured at $|0\rangle_N$ and the number of shots the controlled qubit was measured at 0, that is. We tested this method and Zero Noise Extrapolation on `ibmq-Fez`, one of their most recent quantum computers, on one of the deeper circuits, for multiple random parameters. The results obtained are presented in Table 2

The distance d is simply the absolute difference between the ideal result and the obtained value, either through ZNE or depolarizing mitigation. The new mitigation technique was better in every run With the exception of run 6, where the ideal result was 0. This is to be expected given that depolarizing noise in a Hadamard test has an expectation value of zero, meaning that in this case this kind of noise does not change the measurement.

The obtained factors $1-\lambda$ are also plotted in Fig. 9. With the exception of run 2, we can see that the values are always around 0.43, which demonstrate that the this method is robust against different system calibrations and temporal drifts.

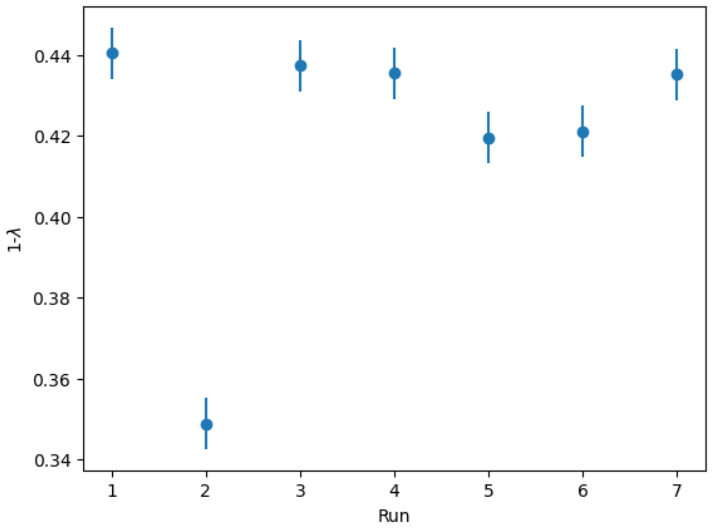

Figure 9: Different values of $1-\lambda$ obtained for different random parameters

This project receives funding from the European Union's Horizon 2020 HORIZON Research and Innovation Actions Programme under Grant Agreement #101080085

Run	d_{ZNE}	$d_{\text{Mitigated}}$
1	0.075	0.006
2	0.068	0.032
3	0.057	0.008
4	0.055	0.016
5	0.072	0.024
6	0.009	0.017
7	0.023	0.013

Table 2: Relative distance between the ideal value expected for each run and the value extrapolated via ZNE and the mitigated value, respectively

Data presented here regarding hardware implementation is available at DOI 10.25592/uhhfdm.16718 while the comparison with classical emulation of noisy quantum hardware is provided at 10.25592/uhhfdm.16108.

6.3 Emulation on PlanQC simulator

The simulations are performed by first compiling to the native gate set of planqc's hardware. This gate set comprises global $R_X(\theta) = e^{i\theta X/2}$ rotations, local $R_Z(\theta) = e^{i\theta Z/2}$ rotations and entangling $CZ = \text{diag}(1, 1, 1, -1)$ gates. Any single-qubit unitary U can be decomposed as

$$U(\alpha, \beta, \gamma) = R_Z(\gamma) R_X\left(-\frac{\pi}{2}\right) R_Z(\beta) R_X\left(\frac{\pi}{2}\right) R_Z(\alpha). \tag{16}$$

Note that the two R_X rotations have opposite angles, and thus they can be performed on all atoms simultaneously if the R_Z rotations are performed locally, since they will cancel out on all spectator atoms. Together with the two-qubit entangling operation, this thus forms a universal gate set for quantum computation.

Once the circuits have been decomposed to their native gate set, we then add a circuit-level noise model that is specific to planqc's neutral-atom hardware. After each gate, we therefore introduce an error channel

$$\mathcal{E}(\rho) = \sum_{\alpha} K_\alpha \rho K_\alpha^\dagger, \tag{17}$$

where K_α are the Kraus operators. This noise model has been obtained from simulations of few-atom physics, which includes the finite temperature of the individual atoms, the recoil induced by the laser fields, amplitude and phase noise on the laser fields, and spontaneous decay. For the R_X and CZ gates, we choose three realistic parameter regimes, which we label as 'low', 'medium' and 'high'. These correspond

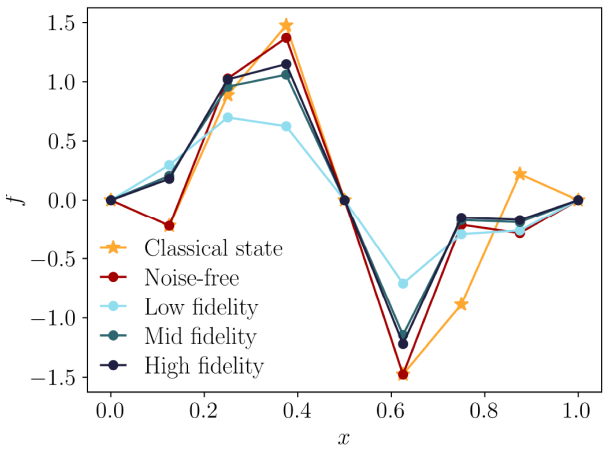

Figure 10: Results from the integration of the Burgers' equation for a time step $dt = 0.3$ with 3 qubits. The solution obtained with an Euler step ('Classical state') is plotted along with the solution obtained using the variational optimization ('Noise-free'). The noisy simulations are compared with different fidelities ('Low', 'Medium' and 'High') of the native gates in the neutral-atom platform.

This project receives funding from the European Union's Horizon 2020 HORIZON Research and Innovation Actions Programme under Grant Agreement #101080085

to fidelities of 99.5 %, 99.8 %, 99.9 % for the R_X gate. and 99.4 %, 99.8 %, 99.9 % for the CZ gate. The R_Z gates have a negligible error rate, since they are physically realized by inducing light shifts on the atoms, which are insensitive to most of the leading sources of error.

In Fig. 10, we show the results obtained from a single integration step of the Burgers' equation for a single time step. Already with a single layer, a relatively good match with the classical time evolution. With the addition of noise, a good overlap with the noise-free solution is achieved already from 'medium' gate fidelities. Data from the simulations can be found at DOI 10.25592/uhhfdm.16690.

Regarding a practical implementation, the circuits can be realized on a neutral atom array with nearest and next-to-nearest neighbor connectivity on a triangular lattice, without requiring swap gates. Furthermore, neutral atom arrays have the potential to natively multi-controlled gates such as CCZ, which could significantly reduce the circuit depth (and thus decrease the error) of the circuits with the adder gadget.

7 European Hardware

The experiments that were successfully run did so via access to the IBMQ cloud devices. Aside from this access, which was already limited and sparse, the main goal of the funding program is rather to create synergies between European hardware and software developers. However, thus far, European hardware that is publicly accessible is still catching up in terms capabilities, and at the time of this report minimum system requirements were not sufficient for running the algorithm even for minimal problem instances. Nonetheless, we expect that in the remaining couple of years that this situation should significantly improve, and we will soon start running the QCFD code on European hardware.

7.1 Experiments planned upon scheduled hardware availability

- As part of the European initiative EuroHPC, as well as other potential routes such as the OpenSuperQ+100 project, we will soon be able to gain access via cloud platforms (e.g. at FZJ) to such providers as IQM, Eleqtron, and Pasqal.
- FZJ in-house devices will also be available via these projects, as well as primarily through the German demonstrator project QSolid, working closely with the QCFD FZJ theory team. The facilities being very young, however, it will slightly lag in availability behind some of the others.
- Via a partnership with TUC, AQT will also offer ion trap quantum processors capable of running the depths and widths of circuits required. This may result in dedicated access which substantially improves throughput.
- Public cloud access to TU Delft QInspire will provide further devices, with several solid state chips slated to become available during the next year.
- Partner PlanQC will offer classical simulators in the short term, with hardware beginning to come online only in the following year.

7.2 Improvement feedback

Through our various tests, attempted runs, and large sweeps of parameter regimes through classical gate-level simulations, there is already a significant know-how that we have gained with respect to implementation of the algorithm. This in turn provides tangible data on areas of needed improvement from which the hardware providers can benefit.

- Long variational optimizations (single execution of the algorithm last at least 200ms) combined long queues on the cloud implies session times should be substantially increased to beyond 16 hours.
- Provided simulators do not accurately capture the role of noise, as evident by the increase of MSE from the expected 0.138 on `ibmq-Sherbrooke` on the report from **workpackage 6.1** to 0.262 in practice. This is partially attibutable to tiling - we increase the number of qubits used beyond our current capabilities to classically simulate them and at the same time are forced to use worst performing qubits;

This project receives funding from the European Union's Horizon 2020 HORIZON Research and Innovation Actions Programme under Grant Agreement #101080085

- One of the main bottlenecks of this and other variational (Hadamard-test) type of algorithms is the very large number of quantum shots to estimate observables, which is only made worse when error mitigations is incorporated. This is especially a problem with readout via fluorescence imaging which takes up a large fraction of the execution time. In general, improved duty cycles and/or better options for dedicated system access would alleviate some of these difficulties.
- Current topologies are not well suited for variational algorithms with Hadamard tests. These are quite often designed for error correcting codes, which are still many years away from overcoming the performance setbacks (from topology or otherwise). Multiply-connected architectures are much more suitable given the standard need for multiply-controlled gates as well as the need to reduce swapping of qubits as much as possible (as it dramatically increases circuit depth).
- The variational circuits require variable angles of rotation for the gates. It should be fairly straightforward to include analog gates in the gate-set, e.g. the fsim gate, rather than construct these from constituent digital gates, since it creates an overhead factor of 2-3.
- Other improvements in gate sets would also be highly beneficial. For example, optimized swapping gates, or the inclusion of CPHASE gates (which are native to most architectures, if not the most efficient) would be very suitable given the large number of controlled operations. Another possible avenue would be to include higher level (e.g. qutrit) gates which is well known to give a significant potential reduction in circuit depths.
- In general, error rates at the fractions of percent level are not low enough for standard circuit sizes, even for demonstration purposes. These should be reduced by a factor of 2-3 to be commensurate with the depths, which should also be achievable via common control theory techniques.

8 Summary

In this report, we have shown first steps towards implementation on quantum hardware, which are presently bottlenecked by the throughput and error rates of the systems. In particular, we have completed systematic noisy emulations of the quantum hardware to determine the prospects of running deep variational circuits on present quantum hardware and based our experiments on these parameter regimes. Thus far, cloud European hardware has been very sparse, but we have successfully run instances of the Nonlinear Schrödinger equation and of the Burgers' equation on IBMQ, albeit with quite noisy circuits, even when compared to the noisy emulation. Our investigation has established the principle areas for improvement that are needed for increasing prospects of running NISQ era variational algorithms on European hardware.

This project receives funding from the European Union's Horizon 2020 HORIZON Research and Innovation Actions Programme under Grant Agreement #101080085

References

[1] Lawrence C Evans. *Partial differential equations*, volume 19. American Mathematical Society, 2022.

[2] Gordon D Smith. *Numerical solution of partial differential equations: finite difference methods*. Oxford university press, 1985.

[3] Frank Arute, Kunal Arya, Ryan Babbush, Dave Bacon, Joseph C. Bardin, Rami Barends, Rupak Biswas, Sergio Boixo, Fernando G. S. L. Brandao, David A. Buell, Brian Burkett, Yu Chen, Zijun Chen, Ben Chiaro, Roberto Collins, William Courtney, Andrew Dunsworth, Edward Farhi, Brooks Foxen, Austin Fowler, Craig Gidney, Marissa Giustina, Rob Graff, Keith Guerin, Steve Habegger, Matthew P. Harrigan, Michael J. Hartmann, Alan Ho, Markus Hoffmann, Trent Huang, Travis S. Humble, Sergei V. Isakov, Evan Jeffrey, Zhang Jiang, Dvir Kafri, Kostyantyn Kechedzhi, Julian Kelly, Paul V. Klimov, Sergey Knysh, Alexander Korotkov, Fedor Kostritsa, David Landhuis, Mike Lindmark, Erik Lucero, Dmitry Lyakh, Salvatore Mandrà, Jarrod R. McClean, Matthew McEwen, Anthony Megrant, Xiao Mi, Kristel Michielsen, Masoud Mohseni, Josh Mutus, Ofer Naaman, Matthew Neeley, Charles Neill, Murphy Yuezhen Niu, Eric Ostby, Andre Petukhov, John C. Platt, Chris Quintana, Eleanor G. Rieffel, Pedram Roushan, Nicholas C. Rubin, Daniel Sank, Kevin J. Satzinger, Vadim Smelyanskiy, Kevin J. Sung, Matthew D. Trevithick, Amit Vainsencher, Benjamin Villalonga, Theodore White, Z. Jamie Yao, Ping Yeh, Adam Zalcman, Hartmut Neven, and John M. Martinis. Quantum supremacy using a programmable superconducting processor. *Nature*, 574(7779):505–510, Oct 2019.

[4] Lov K. Grover. Quantum computers can search arbitrarily large databases by a single query. *Phys. Rev. Lett.*, 79:4709–4712, Dec 1997.

[5] M. Cerezo, Andrew Arrasmith, Ryan Babbush, Simon C. Benjamin, Suguru Endo, Keisuke Fujii, Jarrod R. McClean, Kosuke Mitarai, Xiao Yuan, Lukasz Cincio, and Patrick J. Coles. Variational quantum algorithms. *Nature Reviews Physics*, 3(9):625–644, Sep 2021.

[6] John Preskill. Quantum computing in the nisq era and beyond. *Quantum*, 2:79, 2018.

[7] Lars S. Madsen, Fabian Laudenbach, Mohsen Falamarzi. Askarani, Fabien Rortais, Trevor Vincent, Jacob F. F. Bulmer, Filippo M. Miatto, Leonhard Neuhaus, Lukas G. Helt, Matthew J. Collins, Adriana E. Lita, Thomas Gerrits, Sae Woo Nam, Varun D. Vaidya, Matteo Menotti, Ish Dhand, Zachary Vernon, Nicolás Quesada, and Jonathan Lavoie. Quantum computational advantage with a programmable photonic processor. *Nature*, 606(7912):75–81, Jun 2022.

[8] QuEra Computing. Aquila, our 256-qubit quantum processor. `https://www.quera.com/aquila`, May 2023. Accessed: 2023-05-23.

[9] Colin D Bruzewicz, John Chiaverini, Robert McConnell, and Jeremy M Sage. Trapped-ion quantum computing: Progress and challenges. *Applied Physics Reviews*, 6(2), 2019.

[10] Rigetti Computing. Rigetti computing, 2024. Accessed: 2024-09-25.

[11] Ali Javadi-Abhari, Matthew Treinish, Kevin Krsulich, Christopher J. Wood, Jake Lishman, Julien Gacon, Simon Martiel, Paul D. Nation, Lev S. Bishop, Andrew W. Cross, Blake R. Johnson, and Jay M. Gambetta. Quantum computing with Qiskit, 2024.

[12] J. M. Pino, J. M. Dreiling, C. Figgatt, J. P. Gaebler, S. A. Moses, M. S. Allman, C. H. Baldwin, M. Foss-Feig, D. Hayes, K. Mayer, C. Ryan-Anderson, and B. Neyenhuis. Demonstration of the trapped-ion quantum ccd computer architecture. *Nature*, 592(7853):209–213, Apr 2021.

[13] Jens Koch, Terri M. Yu, Jay Gambetta, A. A. Houck, D. I. Schuster, J. Majer, Alexandre Blais, M. H. Devoret, S. M. Girvin, and R. J. Schoelkopf. Charge-insensitive qubit design derived from the cooper pair box. *Phys. Rev. A*, 76:042319, Oct 2007.

[14] V. Bouchiat, D. Vion, P. Joyez, D. Esteve, and M. H. Devoret. Quantum coherence of charge states in the single electron box. *Journal of Superconductivity*, 12(6):789–797, Dec 1999.

[15] G. S. Paraoanu. Microwave-induced coupling of superconducting qubits. *Phys. Rev. B*, 74:140504, Oct 2006.

This project receives funding from the European Union's Horizon 2020 HORIZON Research and Innovation Actions Programme under Grant Agreement #101080085

[16] Chad Rigetti and Michel Devoret. Fully microwave-tunable universal gates in superconducting qubits with linear couplings and fixed transition frequencies. *Phys. Rev. B*, 81:134507, Apr 2010.

[17] A. Wallraff, D. I. Schuster, A. Blais, L. Frunzio, J. Majer, M. H. Devoret, S. M. Girvin, and R. J. Schoelkopf. Approaching unit visibility for control of a superconducting qubit with dispersive readout. *Phys. Rev. Lett.*, 95:060501, Aug 2005.

[18] D. I. Schuster, A. Wallraff, A. Blais, L. Frunzio, R.-S. Huang, J. Majer, S. M. Girvin, and R. J. Schoelkopf. ac stark shift and dephasing of a superconducting qubit strongly coupled to a cavity field. *Phys. Rev. Lett.*, 94:123602, Mar 2005.

[19] P. Krantz, M. Kjaergaard, F. Yan, T. P. Orlando, S. Gustavsson, and W. D. Oliver. A quantum engineer's guide to superconducting qubits. *Applied Physics Reviews*, 6(2):021318, 06 2019.

[20] A. Scott. *Encyclopedia of nonlinear science*. Routledge, New York, 2006.

[21] G. Agrawal. *Nonlinear fiber optics*. 2013.

[22] K. Nakkeeran. Nonlinear waves in atomic media. *Chaos, Solitons & Fractals*, 13:673, 2002.

[23] H. Triki, C. Bensalem, A. Biswas, S. Khan, Q. Zhou, S. Adesanya, S. P. Moshokoa, and M. Belic. Nonlinear optical phenomena. *Optics Communications*, 437:392, 2019.

[24] C. Sulem and P.-L. Sulem. *The nonlinear Schrödinger equation: self-focusing and wave collapse*. Springer Science & Business Media, 1999.

[25] E. P. Gross. Structure of a quantized liquid. *Il Nuovo Cimento (1955-1965)*, 20:454, 1961.

[26] L. P. Pitaevskii. Vortex lines in superfluid he ii. *Sov. Phys. JETP*, 13:451, 1961.

[27] F. Dalfovo, S. Giorgini, L. P. Pitaevskii, and S. Stringari. Theory of bose-einstein condensation in trapped gases. *Reviews of Modern Physics*, 71:463, 1999.

[28] A. J. Leggett. Bose-einstein condensation in the alkali gases: a status report. *Reviews of Modern Physics*, 73:307, 2001.

[29] L. Pitaevskii and S. Stringari. *Bose-Einstein condensation*. 2003.

[30] M. Edwards and K. Burnett. Quantum dynamics of trapped bose gases. *Physical Review A*, 51:1382, 1995.

[31] M. Lubasch, J. Joo, P. Moinier, M. Kiffner, and D. Jaksch. Nonlinear dynamics of light in multimode systems. *Physical Review A*, 101:010301, 2020.

[32] Kristan Temme, Sergey Bravyi, and Jay M. Gambetta. Error mitigation for short-depth quantum circuits. *Phys. Rev. Lett.*, 119:180509, Nov 2017.

[33] Joel J Wallman and Joseph Emerson. Noise tailoring for scalable quantum computation via randomized compiling. *Physical Review A*, 94(5):052325, 2016.

[34] Ewout Van Den Berg, Zlatko K Minev, and Kristan Temme. Model-free readout-error mitigation for quantum expectation values. *Physical Review A*, 105(3):032620, 2022.

[35] Miroslav Urbanek, Benjamin Nachman, Vincent R Pascuzzi, Andre He, Christian W Bauer, and Wibe A de Jong. Mitigating depolarizing noise on quantum computers with noise-estimation circuits. *Physical review letters*, 127(27):270502, 2021.

This project receives funding from the European Union's Horizon 2020 HORIZON Research and Innovation Actions Programme under Grant Agreement #101080085